

A Model for Scale Interaction in the Madden–Julian Oscillation*

BIN WANG

International Pacific Research Center, and Department of Meteorology, University of Hawaii at Manoa, Honolulu, Hawaii

FEI LIU

International Pacific Research Center, University of Hawaii at Manoa, Honolulu, Hawaii

(Manuscript received 2 September 2010, in final form 28 June 2011)

ABSTRACT

The Madden–Julian oscillation (MJO) is an equatorial planetary-scale circulation system coupled with a multiscale convective complex, and it moves eastward slowly (about 5 m s^{-1}) with a horizontal quadrupole vortex and vertical rearward-tilted structure. The nature and role of scale interaction (SI) is one of the elusive aspects of the MJO dynamics. Here a prototype theoretical model is formulated to advance the current understanding of the nature of SI in MJO dynamics. The model integrates three essential physical elements: (a) large-scale equatorial wave dynamics driven by boundary layer frictional convergence instability (FCI), (b) effects of the upscale eddy momentum transfer (EMT) by vertically tilted synoptic systems resulting from boundary layer convergence and multcloud heating, and (c) interaction between planetary-scale wave motion and synoptic-scale systems (the eastward-propagating super cloud clusters and westward-propagating 2-day waves). It is shown that the EMT mechanism tends to yield a stationary mode with a quadrupole vortex structure (enhanced Rossby wave component), whereas the FCI yields a relatively fast eastward-moving and rearward-tilted Gill-like pattern (enhanced Kelvin wave response). The SI instability stems from cooperative FCI or EMT mechanisms, and its property is a mixture of FCI and EMT modes. The properties of the unstable modes depend on the proportion of deep convective versus stratiform/congestus heating or the ratio of deep convective versus total amount of heating. With increasing stratiform/congestus heating, the FCI weakens while the EMT becomes more effective. A growing SI mode has a horizontal quadrupole vortex and rearward-tilted structure and prefers slow eastward propagation, which resembles the observed MJO. The FCI sets the rearward tilt and eastward propagation, while the EMT slows down the propagation speed. The theoretical results presented here point to the need to observe multcloud structure and vertical heating profiles within the MJO convective complex and to improve general circulation models' capability to reproduce correct partitioning of cloud amounts between deep convective and stratiform/congestus clouds. Limitations and future work are also discussed.

1. Introduction

The Madden–Julian oscillation (MJO) features an equatorially trapped, planetary-scale baroclinic circulation cell (Madden and Julian 1971, 1994) coupled with a multiscale convective complex (Nakazawa 1988) and

propagates eastward slowly (about 5 m s^{-1}) in the Eastern Hemisphere (Knutson and Weickmann 1987). The MJO circulation comprises equatorial Kelvin and Rossby waves and shows a quadrupole vortex horizontal structure when the MJO convection is located over the equatorial Indian Ocean and western Pacific (Rui and Wang 1990; Hendon and Salby 1994). The vertical structure of the MJO is characterized by a boundary layer moisture convergence preceding the major convection region (Hendon and Liebmann 1994; Maloney and Hartmann 1998; Sperber 2003; Tian et al. 2006). The convective complex consists of mesoscale and synoptic disturbances with a variety of cloud types such as deep and shallow convection, stratiform, and congestus clouds (Johnson et al. 1999). The aforementioned

* School of Ocean and Earth Science and Technology Contribution Number 8504 and International Pacific Research Center Publication Number 819.

Corresponding author address: Dr. Bin Wang, IPRC, and Department of Meteorology, University of Hawaii at Manoa, 401 POST Bldg., 1680 East-West Road, Honolulu, HI 96822.
E-mail: wangbin@hawaii.edu

characteristics provide focal points for theoretical interpretations.

Earlier theories of the MJO were built on a direct interaction between large-scale dynamics and bulk parameterization of convective heating, including wave–convective instability of the second kind (CISK) (e.g., Lau and Peng 1987), evaporation–wind feedback (Emanuel 1987; Neelin et al. 1987; Wang 1988a), and boundary layer frictional convergence instability (FCI) or frictional CISK (Wang 1988b; Wang and Rui 1990). Later, cloud–radiation interaction (Hu and Randall 1994; Raymond 2001; Fuchs and Raymond 2005) and convection–moisture feedback (Woolnough et al. 2001; Grabowski and Moncrieff 2004; Raymond and Fuchs 2009) were recognized to play a significant role in maintaining the MJO. These studies, however, did not elaborate the scale interactive processes embedded in the MJO circulation and convective complex.

Recent theoretical studies of the MJO have focused on understanding the roles of the scale interaction (SI) by developing the multiscale models (Majda and Biello 2004, hereafter MB04; Biello and Majda 2005, hereafter BM05; Majda and Stechmann 2009a). It has been demonstrated that the eddy momentum transfer (EMT) generated by the rearward-tilted super cloud clusters (SCCs) may make an MJO-like system (MB04). An improved multiscale model developed by BM05 includes both congestus clouds and SCCs, which are located respectively in the eastern and western part of the convective complex. The BM05 model reproduced a realistic quadrupole vortex structure. These MJO “muscle” models are built on the feedback of synoptic activity on planetary-scale motion but do not include the modulation of MJO on synoptic-scale disturbances. Majda and Stechmann (2009a) studied interaction between zonal mean flow and EMT on the equator without considering earth rotation. The model produced an intraseasonal oscillation in the mean flow but left eastward propagation unexplained.

Majda and Stechmann (2009b) proposed a minimal dynamical model for the MJO “skeleton” through an implicit representation of the lower tropospheric synoptic activity in the thermodynamic equation. The model was able to capture some fundamental features of the skeleton of MJO, such as slow phase speed, a horizontal quadrupole vortex structure, and the wave dispersion relationship. But the effect of the upscale momentum transfer, which was recognized as more important than the eddy heat transfer (MB04), is not explicitly represented in this skeleton model.

The present paper articulates a prototype model for SI in the MJO with an explicit representation of the effects of the EMT by SCCs and 2-day waves and the MJO modulation on these synoptic activities. The present

model integrates three essential physical processes: (a) large-scale FCI of the equatorial waves; (b) effects of upscale EMT by vertically tilted synoptic systems resulting from boundary layer convergence and multicloud (deep convective, stratiform, and congestus clouds) heating; and (c) the interaction between the planetary-scale MJO and SCCs and 2-day waves. Thus, the model describes an instability resulting from the interaction among planetary-scale MJO circulation, boundary layer dynamics, and synoptic disturbances embedded in the MJO convective complex.

2. Physical consideration

The interaction of the equatorial waves, boundary layer dynamics, and collective effects of convective heating is of central importance to large-scale MJO dynamics (Wang 2005). The planetary-scale circulation of MJO involves semigeostrophic, low-frequency equatorial Kelvin and Rossby waves. Observation has established that shallow convection and congestus clouds that moisten and precondition the lower troposphere in front of the deep convection region are organized by planetary boundary layer convergence (Hendon and Salby 1994; Maloney and Hartmann 1998; Sperber 2003; Tian et al. 2006). The moisture convergence in the boundary layer, which is jointly generated by the low-frequency Kelvin and Rossby waves, generates an equatorial heating in the low pressure of the Kelvin wave. This provides a critical mechanism that couples eastward-propagating Kelvin wave and westward-propagating Rossby waves together and selects preferred eastward movement (Wang and Rui 1990). In a basic state that is stable to wave-CISK, the addition of boundary layer convergence-induced heating may provide an instability source, namely frictional convergence instability (Wang 1988b), as does addition of an evaporation–wind feedback mechanism (Emanuel 1987; Neelin et al. 1987; Wang and Li 1994). The FCI does not suffer the short-wave “blow-up” problem because the phase of the boundary layer convergence leads that of the wave convergence and acts to couple the lowest baroclinic mode and the barotropic mode; so the resulting available potential energy conversion to kinetic energy is more effective for long waves (Wang 1988b). The crude representation of the bulk cumulus heating in the FCI model precludes scale interactive processes.

The convective complex, which is coupled with the planetary-scale circulation and brings an active (wet) phase of the MJO, can be viewed as an envelope of myriad multiscale convective systems with multiple-cloud heating involved. The convective systems embedded in the complex can move either eastward (such as convectively coupled Kelvin waves or SCCs) or westward (2-day

waves and squall lines) (Nakazawa 1988; Straub and Kiladis 2003; Haertel and Kiladis 2004; Moncrieff 2004). Both the eastward-propagating moist Kelvin waves and westward-propagating inertio-gravity (WIG) waves have a backward-tilted structure in vertical against its propagation direction. This type of vertical structure is valid for a hierarchy of cloudiness, temperature, and humidity within convectively coupled equatorial waves, from the mesoscale to the MJO scale (Mapes et al. 2006; Kiladis et al. 2009). Observations have shown that these disturbances involve multicloud structure: a deep convection core preceded by shallow convection/congestus clouds and tailed by upper tropospheric stratus clouds (Lin and Johnson 1996; Johnson et al. 1999; Houze et al. 2000; Mapes et al. 2006). The impact of the multicloud heating on high-frequency disturbances may produce instability (Kuang 2008) and vertically tilted structures (Khouider and Majda 2006, 2007).

Another key factor responsible for this generic backward tilt is the planetary boundary layer convergences that lead the free tropospheric wave convergence and vertical motion. Figure 1 shows such examples for the eastward-propagating Kelvin waves and westward-propagating inertio-gravity waves. In general, the steady boundary layer convergence on an equatorial beta plane can be determined by the pressure field associated with the wave motions at the top of the boundary layer (Wang and Li 1994). It can be shown that for other types of equatorial waves the boundary layer convergences also lead the free tropospheric wave convergences. This universality for the equatorial waves is rooted in their intrinsic dynamic structures.

The vertically tilted structures of the mesosynoptic systems allow nonzero EMT from the synoptic disturbances to planetary-scale MJO. On the convective scale, the convective momentum transfer (CMT) is a process that converts convective available potential energy to large-scale horizontal kinetic energy. While the CMT, on average, damps large-scale motions, in the westerly burst regime of the MJO the CMT can transfer momentum to large-scale motion (Tung and Yanai 2002a,b). Moncrieff (2004) proposed that the upscale (i.e., from small to large scale) momentum and heat transfer may play an important role in maintaining the MJO. The theoretical model of MB04 has demonstrated that the upscale EMT induced by SCCs can alter large-scale mean flows and generate planetary-scale features that look like the MJO.

On the other hand, the synoptic wave activity is organized by large-scale equatorial wave convergences. As such, the interaction between planetary-scale circulation and synoptic convective systems is potentially a critical process involved in the MJO.

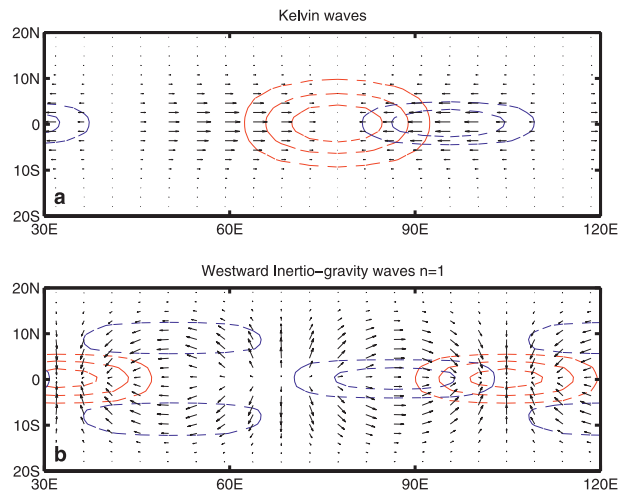


FIG. 1. The relationship between the free tropospheric wave convergence (red contour) and the boundary layer convergence (blue contour) for (a) eastward-propagating equatorial Kelvin waves and (b) westward-propagating inertio-gravity waves ($n = 1$) of zonal wavenumber 5. Only the negative contours are plotted. Vectors represent lower tropospheric winds.

Based on these contemplations, an effort is made in the present study to formulate a new SI model to advance our understanding of essential MJO dynamics. The SI model consists of a boundary layer FCI that mimics the planetary-scale component of the MJO and an explicit representation of EMT effects based on the MB04 and BM05 models. The FCI controls the locations and regulates the strength of the EMT, which in turn feeds back to the FCI by upscale westerly/easterly momentum transfer.

3. The model formulation

a. The dynamic framework for low-frequency planetary-scale motions

Large-scale hydrostatic motion in the tropics can be described by the following primitive equations written on equatorial β -plane and vertical pressure P coordinates:

$$U_t - \beta YV + \Phi_X = F^U - dU, \quad (1)$$

$$\beta YU + \Phi_Y = 0, \quad (2)$$

$$T_t - \frac{P}{R} SW = \frac{Q}{C_p} + F^T - dT, \quad (3)$$

$$\Phi_P = -\frac{RT}{P}, \quad (4)$$

$$U_X + V_Y + W_P = 0, \quad (5)$$

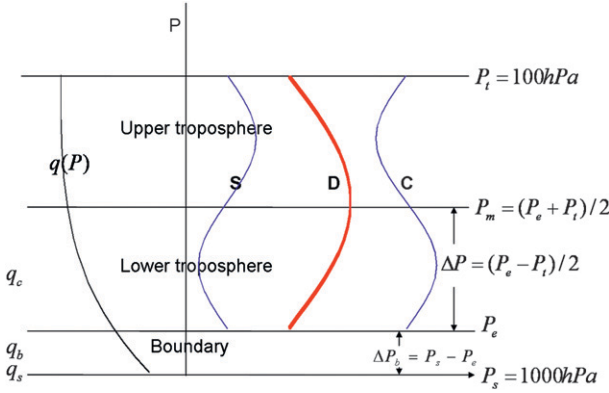


FIG. 2. Schematic diagram describing the model vertical structure, the vertical profile of the basic state specific humidity $q(P)$, and the heating profiles associated with the stratiform (S), deep convective (D), and congestus (C) clouds, respectively.

where (U, V, W) denote the zonal X and meridional Y winds and vertical pressure P velocity, respectively; T and Φ are the temperature and geopotential height; $R = 287 \text{ J kg}^{-1} \text{ K}^{-1}$ is the specific gas constant; $C_p = 1004 \text{ J kg}^{-1} \text{ K}^{-1}$ is the specific heat at constant pressure; and $S = (T/\theta)(\partial\theta/\partial P)$ is the static stability parameter. For simplicity, the momentum and thermal damping coefficients take the same value d in the free troposphere. The terms F^U and F^T are respectively momentum and heat transfer from synoptic systems to planetary-scale motion, and Q is condensation heating rate per unit mass.

The vertical structure of the theoretical model is illustrated in Fig. 2, where P_s , P_e , P_m , and P_t stand for pressure at the surface, the top of boundary layer, the middle troposphere, and the tropopause, respectively. The latent heat released in the deep cumulonimbus clouds warms up the entire tropospheric column with a maximum in the middle troposphere. Cumulus congestus clouds warm up the lower troposphere and cool down the upper troposphere. In contrast, the stratiform clouds warm the upper troposphere and cool the lower troposphere (Khouider and Majda 2006, 2007; Waite and Khouider 2009).

For low-frequency motion, Q can be estimated by steady-state water vapor conservation equation, which links Q to the lower tropospheric moisture convergence \bar{q} (Wang and Rui 1990); that is, $Q = \bar{q}L_q g/\Delta P$ and

$$\bar{q} = \bar{q}_E + \bar{q}_F. \quad (6)$$

In (6), the first term $\bar{q}_E = [(q_b - q_s)/g]W_b$ represents moisture convergence due to the boundary layer Ekman pumping W_b (Wang 1988b); the second term $\bar{q}_F = -(1/g) \int_{P_e}^P \nabla \cdot [q(P)\mathbf{V}] dP$ represents the lower tropospheric moisture convergence. Also, $L_q = 2.5 \times 10^6 \text{ J kg}^{-1}$ denotes the latent heat of condensation, g the gravity,

ΔP the half pressure depth of the free troposphere, and \mathbf{V} horizontal velocity; q_b and q_s stand for mean specific humidity of the boundary layer and the lower troposphere, respectively (Fig. 2), which can be calculated from mean state moisture profile $q(P)$ that is assumed to decrease upward exponentially from q_s at the surface with an e -folding scale (water vapor density scale height) of 2.2 km (Wang 1988b). The basic-state surface specific humidity is estimated based on an empirical dependence on sea surface temperature (SST): $q_s = (0.972\text{SST} - 8.92) \times 10^{-3}$ (Li and Wang 1994). In this study, SST is taken a constant value of 28°C at the equator and decays exponentially poleward with an e -folding scale of 15° of latitude. Therefore, the condensational heating rate is determined by the lower tropospheric and boundary layer moisture convergence and vertical distribution of specific humidity (or SST). The values of constant parameters in (1)–(5) are $S = 3 \times 10^{-6} \text{ m}^2 \text{ s}^{-2} \text{ Pa}^{-2}$, $P_s = 1000 \text{ hPa}$, and $P_t = 100 \text{ hPa}$. The choice of P_e value can switch on/off the boundary layer dynamics and automatically adjust the layer depths. Other parameters are listed in Table 1.

The Ekman pumping at the top of the boundary layer was derived from the steady boundary layer momentum equation for the low-frequency motion (Wang and Li 1994):

$$-\beta Y V_b = -\Phi_{bX} - E U_b, \quad (7)$$

$$\beta Y U_b = -\Phi_{bY} - E V_b. \quad (8)$$

The variables Φ_b , U_b , and V_b denote the geopotential height and zonal and meridional velocity in the barotropic boundary layer, and E is a damping coefficient; Φ_b is assumed to equal the geopotential perturbation in the lower troposphere. The Ekman pumping velocity can be obtained from (7) and (8):

$$W_b = \Delta P_b (d_1 \nabla^2 \Phi_b + d_2 \Phi_{bX} + d_3 \Phi_{bY}), \quad (9)$$

where $d_1 = E/(E^2 + \beta^2 Y^2)$, $d_2 = -\beta(E^2 + \beta^2 Y^2)/(E^2 + \beta^2 Y^2)^2$, and $d_3 = -2E\beta^2 Y/(E^2 + \beta^2 Y^2)^2$. For simplicity, we focus on the equatorial region where $E \gg \beta Y$, so $d_1 = 1/E$, $d_2 = -\beta/E^2$ and $d_3 = 0$.

b. Parameterization of the EMT

The eddy forcing terms in (1) and (3), F^U and F^T , are, respectively, momentum and heat transfer from synoptic systems to planetary-scale motion. Since the heat transfer is only about $1/7$ of the momentum transfer (MB04), only momentum transfer $F^U = -(\overline{UV})_Y - (\overline{UW})_P$ is included.

Based on the assumption that (a) synoptic-scale motions satisfy the weak temperature gradient assumption

TABLE 1. List of the SI model parameters for wavenumber 1. The values listed here were used in the numerical computation unless otherwise noted. Parameters not listed here take the same values as in the standard case (Wang 1988b).

Parameter	Description	Value
β	Meridional variation of the Coriolis parameter	$2.3 \times 10^{-11} \text{ m}^{-1} \text{ s}^{-1}$
C_0	Gravity wave speed of the gravest baroclinic mode	49 m s^{-1}
d	Momentum and heat damping (dimensional) coefficient in the free troposphere	$3 \times 10^{-7} \text{ s}^{-1}$
E	Ekman damping coefficient	$3 \times 10^{-5} \text{ s}^{-1}$
ϕ_0	Spatial lag between stratiform and deep convective heating	$\frac{\pi}{4}$
α	Ratio of deep convective heating to total heating	1–0.5
A	Dimensional amplitude of the EMT	$0.1 \sin(\phi_0) \text{ m s}^{-2}$
ΔP_b	Depth of the boundary layer	$P_s - P_e$
q_c	Mean specific humidity in the lower free troposphere	$\frac{1}{\Delta p} \int_{P_m}^{P_e} q(P) dP$
q_b	Mean specific humidity in the boundary layer	$\frac{1}{\Delta p_b} \int_{P_e}^{P_s} q(P) dP$
c_1	Constant associated with EMT	$\frac{4A \sin(\phi_0)}{3\pi C_0 \sqrt{\beta C_0}}$
c_2	Constant associated with boundary layer moisture convergence	$\frac{\sqrt{\beta C_0} \Delta p_b (q_b - q_c)}{E P_M C_0^2 C_p} \frac{L_q R}{C_0^2 C_p}$
c_3	Constant associated with lower tropospheric moisture convergence	$\frac{\Delta P}{P_M} \frac{L_q R}{q_c C_0^2 C_p}$

(Majda and Klein 2003), (b) synoptic heating involves two vertical modes, deep convective [$\sin(z)$] and stratiform [$\sin(2z)$] (Fig. 2), and (c) the stratiform heating lags deep convective heating by a spatial phase ϕ_0 . MB04 and BM05 derived the upscale momentum transfer for the supercluster system, which can be written under the P coordinate:

$$F^U = \frac{1}{2} A F(X)^2 \alpha (1 - \alpha) V_{er}(P) M(Y). \quad (10)$$

Here A represents the dimensional amplitude, which is controlled by $\sin(\phi_0)$, the tilt of the supercluster (MB04). Also, $F(X)$ is the zonal envelope function of the synoptic scale motions, and its structure will be described in the SI model; α stands for the relative strength of deep convective to the total heating. The strength of the stratiform and congestus heating are assumed to be equal [i.e., $(1 - \alpha)/2$]. The amplitude of the EMT is thus $\alpha(1 - \alpha)/2$. The vertical structure $V_{er}(P) = \cos[(P_e - P)/(P_e - P_t)\pi] - \cos[3(P_e - P)/(P_e - P_t)\pi]$ results from interaction between the stratiform and deep convective heating. Finally, $M(Y) = 2H^2 + YHH_Y$, with $H = e^{-2Y^2}$ denoting meridional structure of synoptic waves.

c. The SI model

In the present model, two types of synoptic systems are considered to interact with the MJO: eastward-propagating SCCs and westward-propagating 2-day waves (or the WIG waves), as observed by Nakazawa (1988). The interaction between the planetary-scale MJO (represented by FCI) and synoptic disturbances is illustrated

schematically in Fig. 3. Based on observations, the eastward-propagating SCCs tilt westward with height (“rearward tilt” with respect to the MJO) (Kiladis et al. 2009), while the westward-propagating 2-day waves tilt eastward with height (“frontward tilt” with respect to the MJO) (Takayabu et al. 1996; Haertel and Kiladis 2004).

The SCCs involve heavy precipitation and fully developed deep convection and stratiform clouds, which show a westward tilt in the Rossby-gyre region of the active MJO (Moncrieff and Klinker 1997; Houze et al. 2000). These observations suggest that the westward tilted SCCs tend to be located in the western part of the convection center. Moreover, the MJO has multicloud structure: shallow convection/congestus clouds are located to the east and stratiform clouds to the west of the deep convections (Kiladis et al. 2009). Because SCCs involve deep convection and stratiform clouds, they must prevail in the central and western part of the MJO. Therefore, we assume that SCCs prevail in the rear part of the MJO convective complex (Fig. 3).

On the other hand, the westward-propagating 2-day waves are assumed to prevail in the front part of the MJO convective complex. Biello and Majda (BM05) used the same assumption. Unfortunately, there was no observational support at that time. In a recent study, Kikuchi and Wang (2010) used spatial-temporal (2D) wavelet transform to detect the nonstationary wave propagation signals from a time-space domain of outgoing longwave radiation (OLR) and found that the enhanced 2-day waves occur to the east of the MJO convective center (i.e., in the front part of the MJO convective

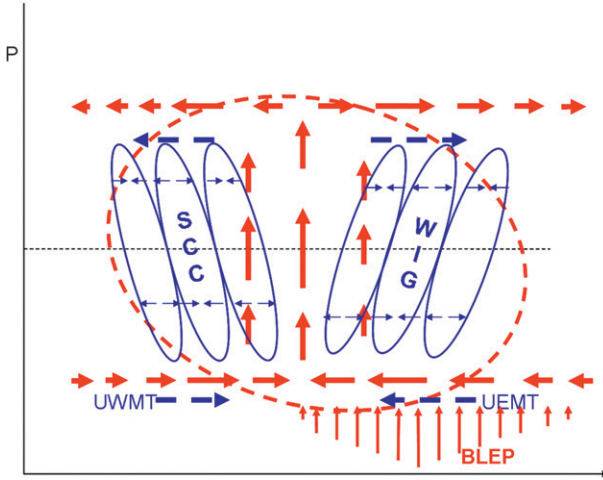


FIG. 3. Schematic diagram describing multiscale structure associated with the model MJO. The red ellipse and thick arrows represent, respectively, the convective complex and planetary-scale zonal circulations associated with the MJO. The blue ellipses and thin arrows denote vertically tilted mesosynoptic disturbances (SCCs and WIG waves) and associated convergence/divergence, respectively. The thick blue arrows represent eddy-induced upscale easterly/westerly momentum transfer (UEMT/UWMT). The red thin arrows represent the boundary layer Ekman pumping (BLEP).

complex). This observed evidence lends support to our assumption and Biello and Majda's assumption.

With the multiscale structure shown in Fig. 3, the SCCs in the rear part of the MJO complex can generate upscale lower tropospheric westerly momentum flux represented by (10). On the other hand, the frontward-tilted 2-day waves can generate upscale lower tropospheric easterly momentum flux:

$$F^U = -\frac{1}{2}AF(X)^2\alpha(1-\alpha)V_{er}(P)M(Y). \quad (11)$$

Thus, the upscale easterly/westerly momentum transfer occurring in the front/rear portion of the convective complex is in phase with the MJO easterly/westerly in the lower troposphere (Fig. 3). As such, (10) and (11) can be combined into one equation:

$$F^U = \frac{1}{2} \text{sgn}[U(X, Y, P, t)]AF(X)^2\alpha(1-\alpha)V_{er}(P)M(Y). \quad (12)$$

The use of the $\text{sgn}(U)$ function in (12) does not mean the zonal wind physically controls the types of synoptic waves or their EMT. A number of factors may be indicative of the types of synoptic waves that may occur in the MJO envelope, such as the lower tropospheric mean zonal flow, the moisture gradient, and the types of boundary layer convergence. The use of zonal wind as an

indicator is not unique, but convenient. The amplitude of EMT is mainly controlled by $F(X)^2$. The $\text{sgn}(U)$ function was used to signify the relative locations of occurrence for the SCCs and 2-day waves with respect to the convective complex center. Note that if $\text{sgn}(U)$ was used alone, a discontinuity occurs at the MJO center, where $U = 0$. This singularity would cause computational difficulty. To overcome this we adopted $U/|U|_{\max}$ to replace $\text{sgn}(U)$, where $|U|_{\max} = \max_{X,Y}(|U(X, Y, P, t)|)$. Equation (12) then becomes

$$F^U = \frac{1}{2} \frac{U(X, Y, P, t)}{|U(X, Y, P, t)|_{\max}} AF(X)^2\alpha(1-\alpha)V_{er}(P)M(Y), \quad (13)$$

where $U/|U|_{\max} > 0$ for westerly and $U/|U|_{\max} < 0$ for easterly.

This first-order parameterization renders $\text{EMT} = 0$ at the MJO center and yields a smooth transition from the SCC-induced EMT to the 2-day wave-induced EMT across the MJO center ($U = 0$). Physically this smooth transition is more reasonable than a “jump” and computationally it overcomes the difficulty caused by the singularity. This parameterization functions as a smoother for the EMT near the MJO center. The results calculated from $\text{sgn}(U)$ with an artificial smoother near the convective complex center have similar results to those calculated with this first-order approximation.

To couple the FCI and EMT mechanisms, it is assumed that \bar{q}_F determines the location and strength of synoptic disturbances; meanwhile, the synoptic systems feed back to the large-scale motions through upscale easterly/westerly momentum transfer. Hence the zonal structure of F^U in (13), $F(X)^2 = \bar{q}_F$; here the square term was used to keep the SI instability at the same order of magnitude as the FCI. The meridional structure of F^U can also be represented by that of the \bar{q}_F , and thus the idealized meridional function $M(Y)$ in (13) is no longer necessary. Now (13) becomes

$$F^U = \frac{1}{2} \frac{U(X, Y, P, t)}{|U(X, Y, P, t)|_{\max}} A\alpha(1-\alpha)V_{er}(P)\bar{q}_F. \quad (14)$$

Although U has a planetary scale, the normalized U only determines the direction of EMT. It is \bar{q}_F that determines the amplitude of EMT, so the moisture convergence supports the growth in its convective envelope. In building the SI model, the meridional structure of EMT is assumed to be determined by the moisture convergence, and $|U(X, Y, P, t)|_{\max} = \max_X(|U(X, 0, P, t)|)$ is defined along the equator.

The large-scale motion in the free troposphere is dominated by the first baroclinic mode. For simplicity,

we project the vertical structures of EMT to the first baroclinic mode in a two-level model and assume that the convergent moisture produces diabatic heating on the first baroclinic mode. Keep in mind that the first baroclinic mode of temperature and deep convective heating all have a maximum at the middle troposphere P_m . The upscale EMT (14) that is projected to the first baroclinic mode can be simplified as $F_1^U \approx 4U_1 A \alpha (1 - \alpha) \bar{q}_{F1} / (3\pi |U_1|_{\max})$. We can simplify \bar{q}_{F1} from (6) as $-\Delta P q_c (U_{1x} + V_{1y}) / g$, where the subscript 1 denotes the first baroclinic mode.

Using characteristic velocity scale $C_0 = \sqrt{S \Delta p^2 / 2} \approx 49 \text{ m s}^{-1}$ (the gravest internal gravity wave speed; Wang 1988b), length scale $L_c = \sqrt{C_0 / \beta} \approx 1460 \text{ km}$, time scale $T_c = 1 / \sqrt{\beta C_0} = 0.34 \text{ day}$, and geopotential height scale C_0^2 , a dimensionless governing equation for the SI model becomes

$$U_{1t} - YV_1 + \Phi_{1X} = c_1 \frac{U_1(X, 0, t)}{|U_1(X, 0, t)|_{\max}} \alpha (1 - \alpha) \bar{q}_{F1} - dU_1, \quad (15)$$

$$YU_1 + \Phi_{1Y} = 0, \quad (16)$$

$$\Phi_{1t} + (U_{1X} + V_{1Y}) = -\alpha (\bar{q}_{E1} + \bar{q}_{F1}) - d\Phi_1, \quad (17)$$

$$\bar{q}_{E1} = c_2 (\nabla^2 \Phi_1 - \Phi_{1X}), \quad (18)$$

$$\bar{q}_{F1} = -c_3 (U_{1X} + V_{1Y}), \quad (19)$$

where the nondimensional coefficients c_1 , c_2 , and c_3 and all other parameters are explained in Table 1. The terms involving c_1 , c_2 , and c_3 denote, respectively, the magnitudes of the EMT, the boundary layer moisture convergence, and the lower tropospheric moisture convergence.

In terms of model parameters, three distinct dynamic regimes can be identified: 1) a pure FCI regime with $P_e < P_s$ (presence of boundary layer) and $\alpha = 1$ (i.e., only deep convective cloud is present, and the EMT vanishes because the absence of vertical tilt of synoptic systems); 2) a pure EMT regime with $P_e < P_s$, and $c_2 = 0$, which means the absence of the BL frictional convergence (or FCI), in which case the solution corresponds to a pure EMT regime if $\alpha < 1$; and 3) an SI regime with $\alpha < 1$ and $c_2 > 0$, which represents a general case involving both FCI and EMT mechanisms.

The SI model (15)–(19) was solved as an initial value problem. The initial perturbation was a small-amplitude, equatorial Kelvin wave convection centered at 90°E —that is, $U_1 = -0.2 \sin[\pi(X - X_0)/X_i] e^{-(Y/Y_L)^2}$ and $U_1 = 0$ when $|X - X_0| > X_i$, where $X_0 = 90^\circ\text{E}$, $X_i = 30^\circ$, and $Y_L = 10^\circ$. In the present model, only a single vertical mode

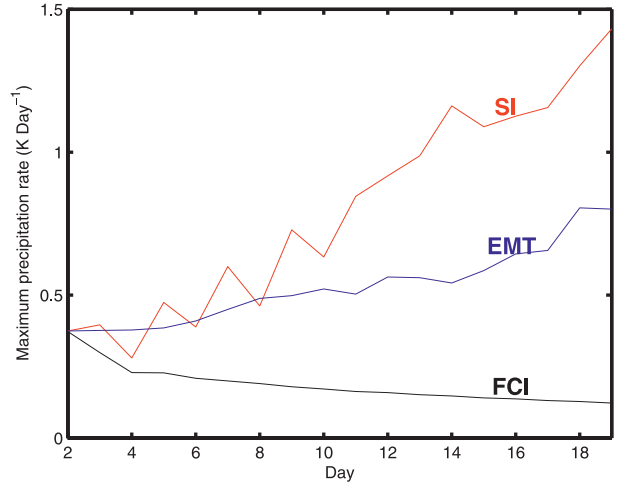


FIG. 4. Maximum heating rate as a function of time for three modes: SI, FCI, and EMT. Here $\alpha = 0.6$.

was considered and the role of the barotropic mode is neglected. This simplification removed the scale selection mechanism elaborated by Wang (1988b). To suppress the fast growth of short waves, the spectral expansion technique (Majda 2003) is used to solve the equations, and only waves with wavenumber smaller than 5 are included. The time step is 4 min. The zonal boundary condition is periodic and no fluxes of mass, momentum, and heat are applied at the meridional lateral boundaries of 30°N and 30°S .

The growths of these three modes are demonstrated in Fig. 4, and we assume that any prediction variable G can be written as $G = G_0 e^{\bar{g}_r t}$, where \bar{g}_r is the averaged growth rate (averaged from day 2 to day 20), which is defined as

$$\sum_{t=2}^{20} G_2 e^{\bar{g}_r (t-2)} = \sum_{t=2}^{20} G_t. \quad (20)$$

Also, the phase speed P_s is defined as

$$P_s = \frac{\text{Lo}(t_2) - \text{Lo}(t_1)}{t_2 - t_1}, \quad (21)$$

where $t_1 = 2 \text{ day}$ and $t_2 = 20 \text{ day}$ are two different times, and Lo represents the location of the maximum convective heating. Here different selection of t_1 and t_2 does not affect the phase speed.

4. Properties of the SI mode

a. Growth rate

The growth rate of the SI mode is expected to vary with α , which represents the fraction of deep convective versus total heating. In (15) and (17), note that α also

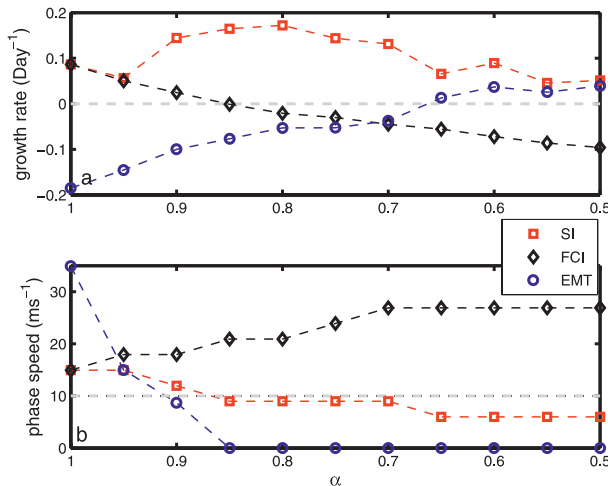


FIG. 5. The properties of the FCI, EMT, and SI modes for wavenumber 1. (a) Growth rate and (b) phase speed as functions of α . Other parameter values used are listed in Table 1.

depicts the proportion of condensational heating that is projected onto the gravest baroclinic mode of FCI and affects the strength of EMT feedback and the coupling between the FCI and EMT. When the amount of stratiform/congestus clouds equals that of deep convection, α is 0.5. Because the EMT comes from the interaction between deep convective heating with amplitude of α and stratiform/congestus heating with amplitude of $1 - \alpha$, the maximum interaction occurs when both deep convective and stratiform/congestus heating have comparable magnitude (i.e., $\alpha = 0.5$).

Figure 5a shows the growth rate as a function of α for wavenumber 1. The growth rate of FCI mode decreases with decreasing α because when α decreases, the amount of deep convective heating that projected to the FCI mode decreases accordingly, and thus the effective (or gross) static stability of the basic state would increase. As a result, the boundary layer moisture convergence can no longer support an unstable mode. The previous works used the unstable FCI mode as a model analog to MJO with $\alpha = 1$ (Wang 1988b; Wang and Li 1994). Here for the given thermal and momentum damping the FCI modes decay for $\alpha < 0.85$.

In sharp contrast, the growth rate of EMT mode increases with decreasing α , or increasing amount of nondeep convective clouds (Fig. 5a). When $\alpha \geq 0.9$, the EMT mode is strongly damped because the stratiform/congestus cloud heating is too weak to support instability. When the stratiform/congestus heating rate increases, the EMT mode strengthens when $\alpha < 0.7$. For a reference, MB04 used the one-way feedback EMT mode with $\alpha = 0.6$ to explain the “westerly wind burst” process associated with the MJO.

The most interesting feature of Fig. 5a is that the SI mode driven by the interaction between the FCI and EMT produces growing modes regardless of the value of α . The SI mode shows fast growth when $0.7 < \alpha < 0.9$ for which the FCI or EMT mechanism alone produces a damped mode, suggesting that the FCI and EMT interact cooperatively to contribute to the SI instability. When $\alpha = 0.8$, the maximum growth rate reaches 0.18 day^{-1} . This value depends on the thermal and momentum damping parameters used.

b. Eastward propagation

Figure 5b compares propagation speed of these three modes. For the FCI mode, phase propagation is largely controlled by the background effective static stability. When $\alpha = 1$, the effective static stability reaches minimum and the FCI mode moves eastward slowly; but with increasing stratiform/congestus cloud heating, the convective heating projected onto FCI mode decreases, thereby increasing the effective static stability and the phase speed.

On the other hand, in the absence of FCI mechanism, the free tropospheric equatorial waves interact with the EMT mechanism. When $\alpha > 0.85$, the EMT effect is very weak; thus, the phase speed is dominated by the eastward-propagating dry Kelvin wave, resulting in a fast propagation (Fig. 5b). With an increase in the amount of stratiform/congestus clouds (or decreasing α), the EMT mechanism plays an increasingly important role, which slows down the eastward propagation. However, once EMT further increases ($\alpha < 0.85$), the EMT mode becomes a stationary system with a Rossby wave-like structure.

It is interesting that the phase speed of the SI mode follows that of FCI mode when $\alpha = 1$ or 0.9 but then rapidly decreases and remains below 10 m s^{-1} thereafter, indicating that the EMT mechanism has played an effective role in slowing down the eastward propagation. When $\alpha < 0.85$, the instability of the SI mode mainly comes from the coupled eastward FCI mode and the stationary EMT mode. The EMT mode has enhanced Rossby wave responses (Fig. 6b), which can efficiently slow down the eastward propagation of the SI mode. Observed slow propagation often occurs when stratiform/congestus clouds are fully developed. Results shown in Fig. 5b indicate that the phase speed of SI mode is comparable with the observed MJO ($0\text{--}10 \text{ m s}^{-1}$) that has fully developed stratiform/congestus in its convective complex.

c. Horizontal structures

To compare horizontal structures of the three modes generated by different mechanisms, we select $\alpha = 0.6$ for

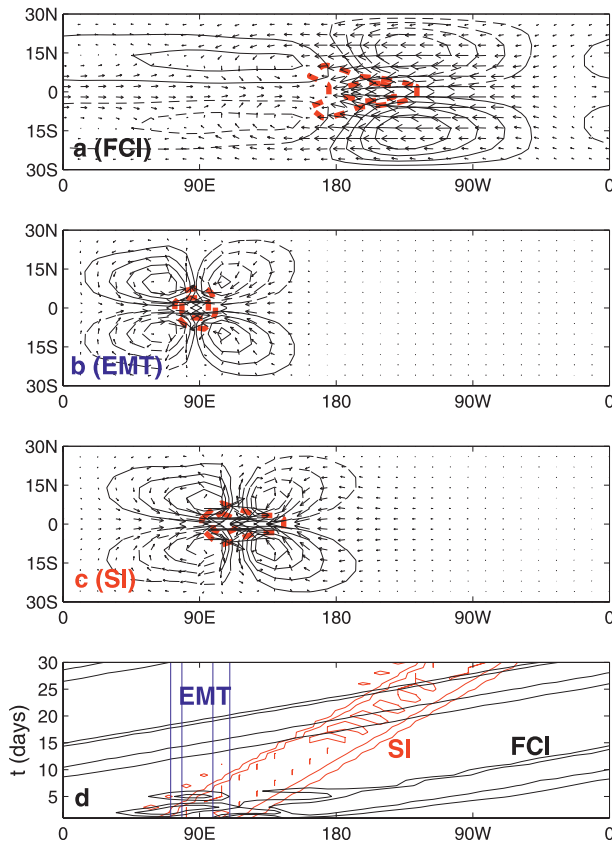


FIG. 6. Horizontal structures of the (a) FCI, (b) EMT, and (c) SI modes for $\alpha = 0.6$ at the seventh day. Shown are planetary-scale winds (vectors) and areas of heating rate (red dashed contour), as well as the streamfunctions (black contours). The vectors and heating rate contours are scaled to their respective maximum magnitudes: (a) 1.5 m s^{-1} , 0.2 K day^{-1} ; (b) 3.7 m s^{-1} , 0.45 K day^{-1} ; and (c) 4.0 m s^{-1} , 0.6 K day^{-1} . (d) Time-longitude diagram of the simulated heating core regions associated with the FCI, EMT, and SI modes. Contour interval is 0.4 for the heating rate and 0.2 for the streamfunctions. Zero contours are not drawn and negative streamfunctions are dashed. The amplitude is a growing function of time.

which the instability of the SI mode comes from the coupled weak FCI and strong EMT modes. The initial disturbance was placed on 90°E . It took a day or so for initial disturbances to adjust (changing horizontal structure and phase speed), so we contrast their evolutions starting from the second day with the same zonal wind amplitude. To facilitate comparison, we aligned the location of the three modes on day 2 at 90°E . Figure 6 compares the lower free tropospheric wind structures of the three modes at day 7. The horizontal structure of damping FCI mode resembles a Gill-like pattern (Gill 1980) with a very weak Rossby wave component (Fig. 6a). The FCI mode moves eastward at a fast speed of about 27 m s^{-1} (Fig. 5b), so on day 7 its center is located at 150°W (Fig. 6d). The horizontal structure is basically

consistent with the previous results (Wang and Li 1994), but the Kelvin wave component has stronger intensity than the Rossby wave component, and thus the equatorial easterlies are too strong compared to the equatorial westerlies. A large portion of the convective region occurs in the lower tropospheric easterly region.

The unstable EMT mode arising from multicloud interaction alone is a stationary Rossby wave-like system at $\alpha = 0.6$ (Figs. 5b and 6b) due to the heating. There is strong convergence between the prominent equatorial westerly and easterly anomalies (Fig. 6b). In off-equatorial regions, a pair of weak anticyclones associated with the equatorial easterlies leads a pair of strong cyclones that are associated with the equatorial westerlies (Fig. 6b). In contrasting to the FCI mode, the EMT mode has an enhanced Rossby wave component at the equatorial westerly region of the MJO.

When the FCI and EMT mechanisms are coupled (i.e., the planetary-scale motion is driven jointly by the FCI and EMT), the unstable SI mode exhibits a horizontal quadrupole vortex structure (Fig. 6c) with a pair of relatively weak anticyclones leading a pair of strong cyclones and propagating eastward at a slow speed of 6 m s^{-1} (Fig. 5b), so that at day 7 the center moves to around 115°E (Fig. 6d). The SI mode has a convective envelope similar to the FCI mode and a quadrupole vortex structure similar to the EMT mode. This mixed structure is consistent with the fact that the SI comes from both FCI and EMT mechanisms (Fig. 5a). The SI mode overcomes the unrealistic structure of the FCI mode (a large portion of convection occurs in the easterly region) and the unrealistic propagation of the EMT mode (stationary), leading to an improved agreement with the observed MJO.

Note also that the results shown in Figs. 5 and 6 are for wavenumber 1, in which a single isolated perturbation is initiated. How do the horizontal structure and phase speed depend on the wavelength? When the parameters used are the same as those for wavenumber 1 the wavenumber-2 SI mode has almost the same horizontal structure and same phase speed as the wavenumber-1 disturbance. For the pure FCI-induced moist Kelvin-Rossby wave packet, the propagation speed of the unstable mode changes from 5 to 15 m s^{-1} (see Fig. 3 of Wang and Rui 1990), which is an unrealistic feature comparing with the observed MJO. With the EMT included, the phase speed of the SI mode does not depend on the wavelength; hence the EMT plays a role in correction of the unrealistic dependence of the phase speed on wavelength for the FCI mode.

The amplitude of the unstable mode shown in Fig. 6 grows forever in time if a fixed high SST is assumed. However, the growth rate is determined by model's

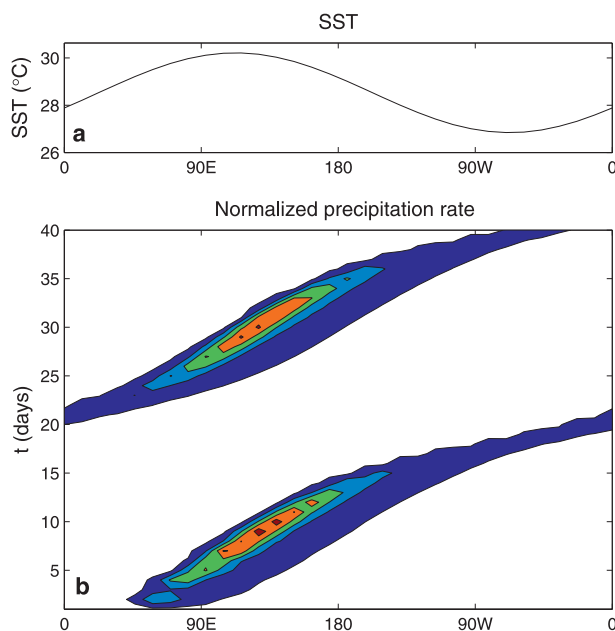


FIG. 7. Evolution of the model SI mode in a longitude-dependent SST setting. (b) A contour plot of normalized heating rate of SI mode calculated from (a) an idealized sinusoidal SST. The maximum heating rate is 0.8 K day^{-1} and contour interval is 0.2 K day^{-1} . Here $\alpha = 0.6$ and initial heating are located at 60°E .

parameters, especially the SST, which controls the magnitude of the moisture convergence and heating rate as it represents the moist static energy sources. In a realistic setting of SST, the MJO-like disturbance will not grow forever. It will grow in the warm-pool ocean region and decay over the cold-tongue regions in the eastern Pacific and Atlantic. This longitudinal dependence behavior of the MJO was demonstrated by Li and Wang (1994). Under an idealized sinusoidal SST (Fig. 7a), the SI mode exhibits a development and slow eastward propagation in the warm ocean region but shows a decay and fast eastward propagation in the cool ocean region (Fig. 7b).

d. The vertical structure

As shown in (6), the condensational heating includes the boundary layer contribution and free tropospheric wave contribution. What is the phase relationship between these two contributions? Figure 8 shows that similar to the FCI model (Fig. 8a) in the SI mode (Fig. 8b), the boundary layer convergence leads the free tropospheric heating because the boundary layer convergence is in phase with the equatorial low pressure (Wang and Li 1994) and the lower tropospheric low pressure leads the free tropospheric convergence (vertical motion). The vertical structure of the SI mode is in good agreement with one of the basic observed properties of the MJO; that

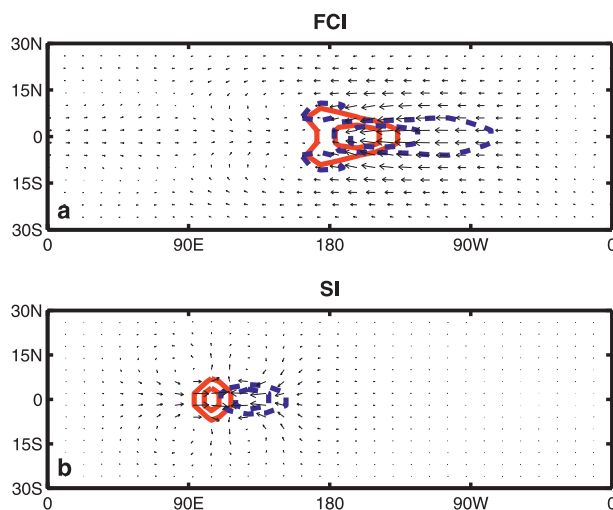


FIG. 8. Relationship between the lower tropospheric (red contours) and boundary layer (blue contours) convergences for the (a) FCI and (b) SI modes. The contour interval is as in Fig. 6. Maximum convective heating (associated with the lower tropospheric and boundary layer convergence) and velocity magnitude are (a) 0.13 K day^{-1} , 0.07 K day^{-1} , 1.5 m s^{-1} and (b) 0.44 K day^{-1} , 0.16 K day^{-1} , 4.0 m s^{-1} .

is, the MJO is characterized by boundary layer moisture convergence preceding major convection region.

5. Concluding remarks

A conceptual model is developed to advance our understanding of scale interaction (SI) dynamics associated with the MJO. The model combines two instability mechanisms. The first results from large-scale wave dynamics driven by the boundary layer frictional convergence instability (FCI) (Wang 1988b; Wang and Rui 1990), and the second is rooted in the eddy momentum transfer (EMT) from synoptic-scale motions to the MJO (MB04; BM05). In this model, the planetary-scale motion controls the location and strength of the synoptic EMT, which in turn feeds back to planetary-scale motion.

We show that the SI instability stems from the combined effect of FCI and EMT mechanisms and thus its property is a mixture of the two modes. The properties of the unstable modes depend on the proportion of deep convective versus stratiform/congestus heating or the ratio of deep convective versus total amount of heating α . When stratiform/congestus heating accounts for only a small portion of the total heating ($\alpha > 0.85$), the FCI produces a growing mode (Fig. 5a), which propagates eastward at a speed of $15\text{--}20 \text{ m s}^{-1}$ (Fig. 5b) and possesses a Gill-like pattern (Fig. 6a) and a backward-tilted structure (Fig. 8a). On the other hand, when the amount of stratiform/congestus clouds increases to a certain

criterion ($\alpha < 0.7$), the EMT generates a growing mode (Fig. 5a) that is stationary (Fig. 5b) and displays a quadrupole vortex pattern (Fig. 6b) without vertical tilt (no boundary layer is included in the EMT mode). The SI instability comes from both the EMT and FCI and possesses fast growth when $0.7 < \alpha < 0.9$ even when the pure FCI or EMT mechanism alone produces a damped mode (Fig. 5a). The SI mode propagates eastward slowly ($5\text{--}10\text{ m s}^{-1}$) and has a mixed structure of the pure EMT and FCI modes—that is, a horizontal quadrupole vortex (Fig. 6c) and backward-tilted structure (Fig. 8b). These properties are equally valid for wavenumber-2 disturbances. Overall, the SI mode resembles the observed MJO in slow eastward propagation, the quadrupole vortex horizontal structure, and the backward-tilted vertical structure, which all are essential features of the MJO.

Because a pure growing EMT mode is stationary, the eastward propagation of the SI mode comes from the contribution of the FCI mechanism, suggesting that the FCI mechanism is essential for selecting the eastward propagation. The FCI also supports the backward-tilted vertical structure. While the EMT mechanism alone does not explain eastward propagation, it favors a quadrupole vortex structure with an enhanced Rossby wave component and plays a critical role in slowing down the eastward propagation of the MJO convective complex.

Numerical experiments with general circulation models (GCMs) have demonstrated that stratiform rains play a critical role in maintaining the MJO and strong MJO exists when stratiform cloud amount exceeds 30% of the deep convection (Fu and Wang 2009). The observation shows that a large portion of stratiform rains exists in mesoscale and synoptic convective systems, which consists of about 40% of all rainfall types in the MJO (Schumacher and Houze 2003). The result of the present theoretical model indicates that the SI mode is favored when the deep convective cloud amount is comparable with stratiform/congestus clouds. Thus, the model result here is consistent with observations and with GCM experimental results.

It is important to note that the positive contribution of the upscale EMT to MJO development depends on the assumed spatial phase relationships between the MJO and the embedded supercluster (occurring in the rear portion of the MJO) and 2-day waves (occurring in the front portion). When the phase relationships change, the corresponding effect of upscale EMT may be different.

The theoretical results here have important ramifications. First, the boundary layer moisture convergence and multicloud heating associated with the equatorial Kelvin and westward-propagating inertio-gravity waves within the convective complex (wet phase) of MJO are

essential for creating vertical tilts of mesosynoptic-scale disturbances or upscale EMT to affect planetary-scale wave dynamics. In this regard, documentation of the vertical heating profiles and multicloud structures should be encouraged. Further, adequate simulation of the MJO in general circulation models may depend on the models' ability to reproduce correct partitioning of the cloud amounts among deep convective and stratiform/congestus clouds. Many GCMs tend to simulate a considerably higher percentage of deep convective clouds compared to the satellite observations. In this case, the EMT mechanism and the SI may be underrepresented.

While EMT can favor a quadrupole vortex structure, this is not the only reason why MJO has such a structure. The quadrupole vortex structure can also be excited, without EMT, by a dipole heating or a wavelike heating as shown by Matsuno (1966). When MJO convection is active over the Indian Ocean, the convection is suppressed over the western Pacific and vice versa. This forms a dipole heating that can stimulate a typical quadrupole vortex structure. Rui and Wang's (1990) composite MJO quadrupole structures were made for these two cases. However, when convective heating is located over the Maritime Continent, the corresponding suppressed convection is weak (although it tends to occur to both sides of the enhanced convection). In this case, the MJO heating is similar to a monopole heating, and a Gill-type pattern is expected as shown by Hendon and Salby (1994).

In this study, a critical assumption made is that SCCs and 2-day waves prevail respectively in the rear and front part of the MJO convection center. While observational evidences support to some degree this assumption, further observational studies are required to clarify the spatial phase relationship among SCCs, 2-day waves, and MJO. In the present SI model, only the first baroclinic mode is considered so that all the moisture convergence produced by the boundary layer Ekman pumping stimulates only the first baroclinic mode. This oversimplified representation neglects the coupling effect of the boundary layer convergence on the vertical modes and cannot favor the long wave growth (Wang 1988b). Inclusion of higher vertical modes in description of EMT mechanism and the role of boundary layer moisture preconditioning would provide a more realistic model for investigating MJO dynamics. We have also assumed a fixed phase lag between the synoptic activity (EMT) and the MJO convective complex and an equal amount of stratiform and congestus clouds, which yields a stationary EMT mode. Further consideration of the wavelength-dependent phase lags and study of the impact on phase propagation of EMT mode under different multicloud structure are warranted.

Acknowledgments. This study is supported by Climate Dynamics Program of the National Science Foundation under Award AGS-1005599 and NASA Award NNX09AG97G. Additional support was provided by the Japan Agency for Marine-Earth Science and Technology (JAMSTEC), by NASA through Grant NNX07AG53G, and by NOAA through Grant NA17RJ1230 through their sponsorship of research activities at the International Pacific Research Center. The lead author thanks Dr. Majda for constructive discussion of aspects of scale interaction involved in MJO dynamics. The authors are grateful to the comments made by three anonymous reviewers, which led to significant improvement of the submitted version of the manuscript.

REFERENCES

- Biello, J. A., and A. J. Majda, 2005: A new multiscale model for the Madden–Julian oscillation. *J. Atmos. Sci.*, **62**, 1694–1721.
- Emanuel, K. A., 1987: An air–sea interaction model of intraseasonal oscillations in the tropics. *J. Atmos. Sci.*, **44**, 2324–2340.
- Fu, X., and B. Wang, 2009: Critical roles of the stratiform rainfall in sustaining the Madden–Julian oscillation: GCM experiments. *J. Climate*, **22**, 3939–3959.
- Fuchs, Z., and D. J. Raymond, 2005: Large-scale modes in a rotating atmosphere with radiative–convective instability and WISHE. *J. Atmos. Sci.*, **62**, 4084–4094.
- Gill, A. E., 1980: Some simple solutions for heat-induced tropical circulation. *Quart. J. Roy. Meteor. Soc.*, **106**, 447–462.
- Grabowski, W. W., and M. W. Moncrieff, 2004: Moisture–convection feedback in the tropics. *Quart. J. Roy. Meteor. Soc.*, **130**, 3081–3104.
- Haertel, P. T., and G. N. Kiladis, 2004: Dynamics of 2-day equatorial waves. *J. Atmos. Sci.*, **61**, 2707–2721.
- Hendon, H. H., and B. Liebmann, 1994: Organization of convection within the Madden–Julian oscillation. *J. Geophys. Res.*, **99**, 8073–8084.
- , and M. L. Salby, 1994: The life cycle of the Madden–Julian oscillation. *J. Atmos. Sci.*, **51**, 2225–2237.
- Houze, R. A., Jr., S. S. Chen, D. E. Kingsmill, Y. Serra, and S. E. Yuter, 2000: Convection over the Pacific warm pool in relation to the atmospheric Kelvin–Rossby wave. *J. Atmos. Sci.*, **57**, 3058–3089.
- Hu, Q., and D. A. Randall, 1994: Low-frequency oscillations in radiative–convective systems. *J. Atmos. Sci.*, **51**, 1089–1099.
- Johnson, R. H., T. M. Rickenbach, S. A. Rutledge, P. E. Ciesielski, and W. H. Schubert, 1999: Trimodal characteristics of tropical convection. *J. Climate*, **12**, 2397–2418.
- Khouider, B., and A. J. Majda, 2006: A simple multicloud parameterization for convectively coupled tropical waves. Part I: Linear analysis. *J. Atmos. Sci.*, **63**, 1308–1323.
- , and —, 2007: A simple multicloud parameterization for convectively coupled tropical waves. Part II: Nonlinear simulations. *J. Atmos. Sci.*, **64**, 381–400.
- Kikuchi, K., and B. Wang, 2010: Spatiotemporal wavelet transform and the multiscale behavior of the Madden–Julian oscillation. *J. Climate*, **23**, 3814–3834.
- Kiladis, G. N., M. C. Wheeler, P. T. Haertel, K. H. Straub, and P. E. Roundy, 2009: Convectively coupled equatorial waves. *Rev. Geophys.*, **47**, RG2003, doi:10.1029/2008RG000266.
- Knutson, T. R., and K. M. Weickmann, 1987: 30–60-day atmospheric oscillation: Composite life cycles of convection and circulation anomalies. *Mon. Wea. Rev.*, **115**, 1407–1436.
- Kuang, Z., 2008: A moisture–stratiform instability for convective coupled waves. *J. Atmos. Sci.*, **65**, 834–854.
- Lau, K. M., and L. Peng, 1987: Origin of low-frequency (intra-seasonal) oscillations in the tropical atmosphere. Part I: Basic theory. *J. Atmos. Sci.*, **44**, 950–972.
- Li, T., and B. Wang, 1994: The influence of sea surface temperature on the tropical intraseasonal oscillation: A numerical study. *Mon. Wea. Rev.*, **122**, 2349–2362.
- Lin, X., and R. H. Johnson, 1996: Kinematic and thermodynamic characteristics of the flow over the western Pacific warm pool during TOGA COARE. *J. Atmos. Sci.*, **53**, 695–715.
- Madden, R., and P. Julian, 1971: Detection of a 40–50-day oscillation in the zonal wind in the tropical Pacific. *J. Atmos. Sci.*, **28**, 702–708.
- , and —, 1994: Observations of the 40–50-day tropical oscillation—A review. *Mon. Wea. Rev.*, **122**, 814–837.
- Majda, A. J., 2003: Waves and PDEs for the equatorial atmosphere and ocean. *Introduction to PDEs and Waves for the Atmosphere and Ocean*, Courant Institute Lecture Series 9, American Mathematical Society, 199–232.
- , and R. Klein, 2003: Systematic multiscale models for the tropics. *J. Atmos. Sci.*, **60**, 393–408.
- , and J. A. Biello, 2004: A multiscale model for tropical intraseasonal oscillations. *Proc. Natl. Acad. Sci. USA*, **101**, 4736–4741.
- , and S. N. Stechmann, 2009a: A simple dynamical model with features of convective momentum transport. *J. Atmos. Sci.*, **66**, 373–392.
- , and —, 2009b: The skeleton of tropical intraseasonal oscillations. *Proc. Natl. Acad. Sci. USA*, **106**, 8417–8422.
- Maloney, E. D., and D. L. Hartmann, 1998: Frictional moisture convergence in a composite life cycle of the Madden–Julian oscillation. *J. Climate*, **11**, 2387–2403.
- Mapes, B. E., S. Tulich, J. Lin, and P. Zuidema, 2006: The mesoscale convection life cycle: Building block or prototype for large-scale tropical waves? *Dyn. Atmos. Oceans*, **42**, 3–29.
- Matsuno, T., 1966: Quasi-geostrophic motions in the equatorial area. *J. Meteor. Soc. Japan*, **44**, 25–43.
- Moncrieff, M. W., 2004: Analytic representation of the large-scale organization of tropical convection. *J. Atmos. Sci.*, **61**, 1521–1538.
- , and E. Klinker, 1997: Organized convective systems in the tropical western Pacific as a process in general circulation models: A TOGA COARE case study. *Quart. J. Roy. Meteor. Soc.*, **123**, 805–827.
- Nakazawa, T., 1988: Tropical super clusters within intraseasonal variations over the western Pacific. *J. Meteor. Soc. Japan*, **66**, 823–839.
- Neelin, J. D., I. M. Held, and K. H. Cook, 1987: Evaporation–wind feedback and low-frequency variability in the tropical atmosphere. *J. Atmos. Sci.*, **44**, 2341–2348.
- Raymond, D. J., 2001: A new model of the Madden–Julian oscillation. *J. Atmos. Sci.*, **58**, 2807–2819.
- , and Z. Fuchs, 2009: Moisture modes and Madden–Julian oscillation. *J. Climate*, **22**, 3031–3046.
- Rui, H., and B. Wang, 1990: Development characteristics and dynamic structure of tropical intraseasonal convection anomalies. *J. Atmos. Sci.*, **47**, 357–379.
- Schumacher, C., and R. A. Houze Jr., 2003: Stratiform rain in the tropics as seen by the TRMM precipitation radar. *J. Climate*, **16**, 1739–1756.

- Sperber, K. R., 2003: Propagation and the vertical structure of the Madden–Julian oscillation. *Mon. Wea. Rev.*, **131**, 3018–3037.
- Straub, K. H., and G. N. Kiladis, 2003: Interactions between the boreal summer intraseasonal oscillation and higher-frequency tropical wave activity. *Mon. Wea. Rev.*, **131**, 945–960.
- Takayabu, Y. N., K. M. Lau, and C. H. Sui, 1996: Observation of a quasi-2-day wave during TOGA COARE. *Mon. Wea. Rev.*, **124**, 1892–1913.
- Tian, B., D. E. Waliser, E. J. Fetzer, B. H. Lambrigtsen, Y. Yung, and B. Wang, 2006: Vertical moist thermodynamic structure and spatial–temporal evolution of the MJO in AIRS observations. *J. Atmos. Sci.*, **63**, 2462–2485.
- Tung, W.-W., and M. Yanai, 2002a: Convective momentum transport observed during the TOGA COARE IOP. Part I: General features. *J. Atmos. Sci.*, **59**, 1857–1871.
- , and —, 2002b: Convective momentum transport observed during the TOGA COARE IOP. Part II: Case studies. *J. Atmos. Sci.*, **59**, 2535–2549.
- Waite, M. L., and B. Khouider, 2009: Boundary layer dynamics in a simple model for convectively coupled gravity waves. *J. Atmos. Sci.*, **66**, 2780–2795.
- Wang, B., 1988a: Comments on “An air–sea interaction model of intraseasonal oscillation in the tropics.” *J. Atmos. Sci.*, **45**, 3521–3525.
- , 1988b: Dynamics of tropical low-frequency waves: An analysis of the moist Kelvin wave. *J. Atmos. Sci.*, **45**, 2051–2065.
- , 2005: Theory. *Intraseasonal Variability of the Atmosphere–Ocean Climate System*. W. K. M. Lau and D. E. Waliser, Eds., Praxis, 307–360.
- , and H. Rui, 1990: Dynamics of the coupled moist Kelvin–Rossby wave on an equatorial beta plane. *J. Atmos. Sci.*, **47**, 397–413.
- , and T. Li, 1994: Convective interaction with boundary layer dynamics in the development of the tropical intraseasonal system. *J. Atmos. Sci.*, **51**, 1386–1400.
- Woolnough, S. J., J. M. Slingo, and B. J. Hoskins, 2001: The organization of tropical convection by intraseasonal sea surface temperature anomalies. *Quart. J. Roy. Meteor. Soc.*, **127**, 887–907.